

Unidirectional transport of wave packets through tilted discrete breathers in nonlinear lattices with asymmetric defects

Xiao-Dong Bai,¹ Boris A. Malomed,² and Fu-Guo Deng^{1*}

¹*Department of Physics, Applied Optics Beijing Area Major Laboratory,
Beijing Normal University, Beijing 100875, China*

²*Department of Physical Electronics, School of Electrical Engineering,
Faculty of Engineering, Tel Aviv University, Tel Aviv 69978, Israel*

(Dated: December 3, 2024)

We consider the transfer of small-amplitude lattice wave packets through a tilted discrete breather (TDB) in opposite directions in the discrete nonlinear Schrödinger model with asymmetric defects, which may be realized as a Bose-Einstein condensate trapped in a deep optical lattice, and as optical beams in a waveguide array. A unidirectional transport mode is found, in which the small-amplitude waves pass the TDB only in one direction, while, in the absence of the TDB, the same lattice admits bi-directional propagation. The operation of this mode is accurately explained by the consideration of respective energy barriers. The results suggest that the TDB may be a diode device candidate, to simulate the diode-like physical phenomena by means of atom and optical beams in the future.

PACS numbers: 63.20.Pw, 03.75.Lm, 05.45.Yv

Time-periodic spatially localized excitations, called discrete breathers (DBs) [1, 2], are supported by diverse nonlinear lattice media, such as arrays of micromechanical cantilevers [3], coupled Josephson junctions [4, 5] and optical waveguides [6–9] (in the latter case, the evolution variable is not time but the propagation distance), anti-ferromagnets [10, 11], Bose-Einstein condensates (BECs) [12–14] and Tonks-Girardeau [15] or superfluid fermionic [16] gases fragmented and trapped in deep optical lattices (OLs), as well as some dissipative systems [17, 18]. DBs provide means for energy concentration and transport in waveguides [19], polaronic materials [20], long biological molecules [21], and other settings [2].

DBs represent attractors in dissipative systems [19, 22, 23], or self-trapped localized modes in conservative nonlinear lattices [24–26]. Collisions of moving solitons or phonons (linear wave packets) with stationary DBs were studied too [25–27]. It was found that, if the amplitude of the incident soliton is too small, it bounces back from the DB. Beyond a specific threshold amplitude, a part of the norm of the incident solitary pulse may be transmitted through the DB. In particular, this transport property is vital for matter-wave interferometry [28] and quantum-information processing [29–32].

Previous works were mainly dealing with symmetric DBs in perfect lattices, the corresponding transfer mechanism being symmetric with respect to the direction of motion of the incident excitation. On the other hand, unidirectional propagation of waves in specially devised systems has drawn much attention too [33]. In particular, it was experimentally demonstrated that a periodically poled waveguide may serve as an optical diode [34]. Further, it was predicted that a combination of a Bragg grating with a periodic lattice built of gain and loss elements

[35], as well as a periodically structured metamaterial [36], a chain of driven ultracold atoms [42], and chains of coupled microcavities [43], may give rise to nonreciprocal light transmission. Starting from early work [37], it was also demonstrated theoretically that photonic crystals (PCs) with edge modes [38], PCs with built-in periodic lattice of defects [39], second-harmonic-generating PCs [40], and quasiperiodic PCs [41], may produce a similar effect. Theoretically predicted and experimentally realized possibilities for the unidirectional light transmission are offered by \mathcal{PT} -symmetric photonic lattices [44]. Asymmetric propagation of microwaves [45] and electric signals [46] was observed, respectively, in appropriately built electromagnetic crystals and electric transmission lines.

Realistic lattices always contain imperfections or defects. In many cases, they dramatically affect the properties of nonlinear lattices, resulting in a number of new phenomena, such as the Anderson localization [47, 48] and the disorder-induced Bose-glass phase [49]. If localized defects have an asymmetric shape, they can asymmetrically deform lattice solitons (alias discrete breathers) pinned to the defects, making them *tilted* discrete breathers (TDBs). In this work, we consider a one-dimensional discrete nonlinear Schrödinger (DNLS) model with an arbitrary level of disorder and demonstrate that, while the underlying lattice admits bi-directional transmission of linear waves, the transmission is made nonreciprocal for waves hitting a pinned TDB in opposite directions. As a result, we find a “diode-like” transport mode, when the incident waves can pass through the TDB only in one direction. Thus, while a localized asymmetric defect cannot directly induce the unidirectional transmission, it may create such a regime with the help of the pinned TDB. This is possible because the scattering of a linear wave on a soliton in a nonlinear system is essentially different from the scattering on a defect in the linear counterpart of the same

*Corresponding author: fgdeng@bnu.edu.cn

system (the linearization of the DNLS around the pinned soliton involves both the linear wave packet and its complex conjugate, thus making the order of the respective scattering problem twice as high). The diode mode can be controlled by varying parameters of the underlying defect.

We start by taking the Bose-Hubbard Hamiltonian, which is the simplest model that captures the dynamics of a dilute gas of bosonic atoms in the deep OL. In the mean-field approximation, the Hamiltonian for the disordered OL is [50]

$$\mathcal{H} = \sum_{n=1}^M \left(\frac{U}{2} |\psi_n|^4 + \epsilon_n |\psi_n|^2 \right) - \frac{J}{2} \sum_{n=1}^{M-1} (\psi_n^* \psi_{n+1} + \text{c.c.}), \quad (1)$$

where n ($= 1, \dots, M$) is the discrete coordinate of the lattice site, ψ_n is the on-site wave function, J is the amplitude of the inter-site hopping, and c.c. stands for the complex conjugate. $U = 4\pi\hbar^2 a_s V_d / m$ is the strength of the collisional on-site interactions, where V_d is the effective mode volume of each site, m is the atomic mass, and a_s is the s -wave atomic scattering length. Here, we consider the case of repulsive interactions, $U > 0$. Lastly, ϵ_n is on-site energy which accounts for the disorder. The scaled DNLS equation following from Hamiltonian (1) is:

$$i \frac{d\psi_n}{dt} = \lambda |\psi_n|^2 \psi_n + \epsilon_n \psi_n - \frac{1}{2} (\psi_{n-1} + \psi_{n+1}), \quad (2)$$

with the normalization is imposed in the form of $\sum_{n=1}^M |\psi_n|^2 = 1$, and scaling defined by $\lambda \equiv U/J$, $\epsilon_n \equiv \epsilon_n/J$, and $t \equiv JT$, where T is time measured in physical units.

In addition to BEC, Eq. (2) applies to the light propagation in arrays of nonlinear optical waveguides [6, 8], with t replaced by the propagation distance (z), λ being the effective Kerr coefficient, and the inter-site coupling coefficient normalized to be 1. In this case, $-\epsilon_n$ is proportional to deviation of the local refractive index from its average value, and $\psi_n(z)$ is the on-site amplitude of the electromagnetic wave in the spatial domain.

The transport of excitations through the DB is mainly determined by the dynamics at three sites on which a narrow DB is located. Therefore, we first address the trimer model ($M = 3$) with system (2) truncated to

$$\begin{aligned} i \frac{d\psi_1}{dt} &= \lambda |\psi_1|^2 \psi_1 + \epsilon_1 \psi_1 - \frac{1}{2} \psi_2, \\ i \frac{d\psi_2}{dt} &= \lambda |\psi_2|^2 \psi_2 + \epsilon_2 \psi_2 - \frac{1}{2} (\psi_1 + \psi_3), \\ i \frac{d\psi_3}{dt} &= \lambda |\psi_3|^2 \psi_3 + \epsilon_3 \psi_3 - \frac{1}{2} \psi_2, \end{aligned} \quad (3)$$

subject to normalization $\sum_{n=1}^3 |\psi_n|^2 = 1$. First, DB solutions are looked for as

$$\psi_n(t) = A_n(t) \exp(-i\mu t), \quad (4)$$

with real amplitudes A_n and chemical potential μ (in optics, $-\mu$ is the propagation constant). It is well known

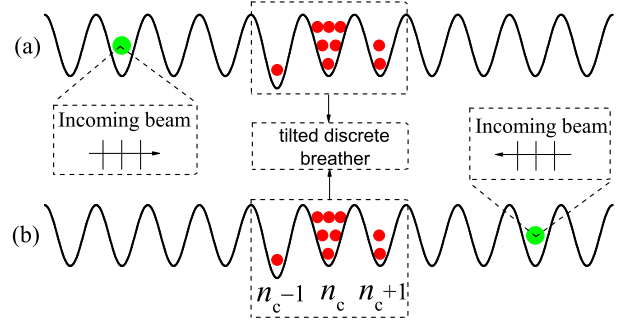


FIG. 1: (Color online) The transport scheme under the consideration. Green large dots denote the same wave packets incoming from the left in (a) and right in (b). The middle part schematically shows the TDB, where $\epsilon_n = 0$, except for $\epsilon_{n_c-1} < 0$.

that localized (self-trapped) discrete modes in the system with the repulsive on-site nonlinearity are possible in the *staggered* form, i.e., with alternating signs of the amplitudes at adjacent sites [2],

$$A_1 > 0, \quad A_2 = -\sqrt{1 - A_1^2 - A_3^2} < 0, \quad A_3 > 0, \quad (5)$$

to comply with the normalization condition. Then, the substitution of Eq. (4) into Eq. (3) for ψ_2 yields

$$\mu = \epsilon_2 + \lambda (1 - A_1^2 - A_3^2) + (A_1 + A_3) / \sqrt{1 - A_1^2 - A_3^2}. \quad (6)$$

As ϵ_2 can be absorbed into a shift of μ in Eq. (6), we set $\epsilon_2 = 0$ below. Two remaining equations for $\psi_{1,3}$ in Eq. (3) are

$$2A_{1,3}[\epsilon_{1,3} + \lambda(2A_{1,3}^2 + A_{3,1}^2 - 1)] = \frac{2A_{1,3}^2 + A_{3,1}^2 + A_1 A_3 - 1}{\sqrt{1 - A_1^2 - A_3^2}}, \quad (7)$$

where μ is eliminated with the help of Eq. (6).

From Eq. (7), one can obtain different types of stationary solutions. For the symmetric configuration with $\epsilon_1 = \epsilon_3$, the stationary states correspond to ordinary symmetric DBs, which have been investigated in detail, including its formation [25, 26] and transport properties [27, 51]. On the other case, the setting with $\epsilon_1 \neq \epsilon_3$ gives rise to TDB, as schematically shown in the middle part of Fig. 1, where $n_c - 1$, n_c , and $n_c + 1$ may be regarded as 1, 2, and 3, respectively, in the trimer model. Here, our aim is to investigate the transport of small-amplitude lattice waves through the TDB, for the wave packets arriving from the opposite directions, see Fig. 1.

Next, we consider the system's Hamiltonian for the DB solutions in the form of Eqs. (4) and (5), which must be taken with the opposite overall sign, due to the staggering transformation:

$$H = -\frac{\lambda}{2} (A_1^4 + A_2^4 + A_3^4) - (\epsilon_1 A_1^2 + \epsilon_3 A_3^2) - (A_1 + A_3) A_2. \quad (8)$$

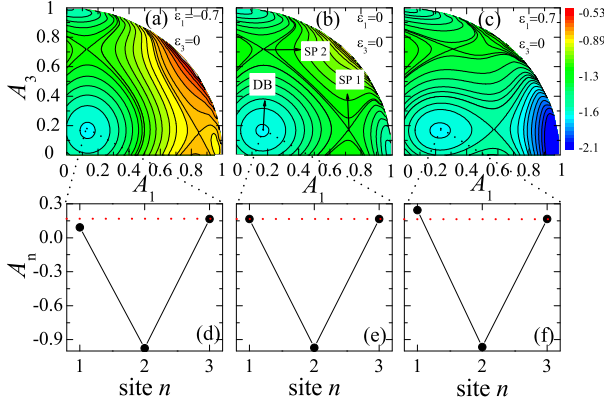


FIG. 2: (Color online) (a)-(c) Contour plots of energy given by Eq. (8) for different ε_1 with fixed $\lambda = 3$ and $\varepsilon_3 = 0$. (d)-(f) The structure of the DB corresponding to panels (a)-(c), respectively. SP1 and SP2 denote the saddle points.

The effect of ε_n on the Hamiltonian, considered as a function of A_1 and A_3 , is shown in Fig. 2(a)-(c), which exhibits three minima separated by two saddle points SP1 and SP2. The minima refer to the DBs, whose structures are displayed in Figs. 2(d)-(f). Analytical solutions for SP1, SP2, and DB can be obtained from Eq. (7) in the limit of large λ and small ε_1 and ε_3 . The respective energies of SP1 and SP2, $E_{\text{thr}1,2}$, which play the role of thresholds for the perturbed dynamics of the trimer (see below), are

$$E_{\text{thr}1} = \frac{1}{2} - \frac{\lambda}{4} - \frac{1}{4\lambda} + \frac{1}{4\lambda^2} - \frac{1}{4\lambda^3} + \frac{9}{16\lambda^4} - \varepsilon_1 \left(\frac{1}{2} + \frac{1}{2\lambda^3} - \frac{5}{8\lambda^4} \right) + \varepsilon_1^2 \left(\frac{1}{4\lambda} + \frac{1}{4\lambda^2} + \frac{1}{16\lambda^3} + \frac{3}{16\lambda^4} \right) - \varepsilon_1^3 \left(\frac{1}{8\lambda^3} + \frac{1}{16\lambda^4} \right) - \varepsilon_3 \left(\frac{1}{2\lambda^2} - \frac{1}{\lambda^3} + \frac{1}{2\lambda^4} \right), \quad (9)$$

$$E_{\text{thr}2} = \frac{1}{2} - \frac{\lambda}{4} - \frac{1}{4\lambda} + \frac{1}{4\lambda^2} - \frac{1}{4\lambda^3} + \frac{9}{16\lambda^4} - \varepsilon_3 \left(\frac{1}{2} + \frac{1}{2\lambda^3} - \frac{5}{8\lambda^4} \right) + \varepsilon_3^2 \left(\frac{1}{4\lambda} + \frac{1}{4\lambda^2} + \frac{1}{16\lambda^3} + \frac{3}{16\lambda^4} \right) - \varepsilon_3^3 \left(\frac{1}{8\lambda^3} + \frac{1}{16\lambda^4} \right) - \varepsilon_1 \left(\frac{1}{2\lambda^2} - \frac{1}{\lambda^3} + \frac{1}{2\lambda^4} \right). \quad (10)$$

In the case of $\varepsilon_1 = \varepsilon_3 = 0$, which corresponds to Fig. 2(b), the discrete solitons corresponding to SP1, SP2, and the DB are symmetric, as shown in Fig. 2(e). On the other hand, an asymmetric setting, with $\varepsilon_3 = 0$ and $\varepsilon_1 = -0.5$, is represented by Fig. 2(a). In this case, the discrete soliton becomes a TDB, shown in Fig. 2(d), where the norm (alias power, in terms of optics) localized at site 1 is smaller than in the symmetric case. SP2 remains nearly the same one as that in the symmetric case, while SP1 moves away from the TDB. The relationship between energy thresholds in this case is $E_{\text{thr}1} > E_{\text{thr}2}$. Similarly, we set $\varepsilon_3 = 0$ and $\varepsilon_1 = 0.5 > 0$ in Fig. 2(c),

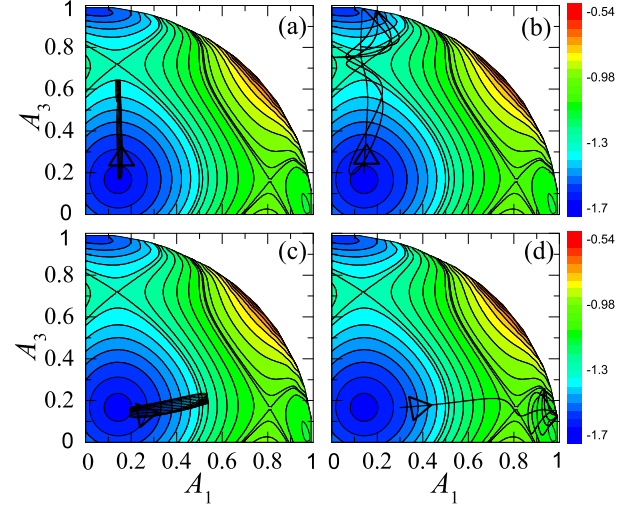


FIG. 3: (Color online) Dynamics of the trimer initiated by the perturbations applied at site 3 (a,b) or at site 1 (c,d). Here $E_{\text{thr}1} = -1.01787 > E_{\text{thr}2} = -1.29859$ correspond to SP1 and SP2, respectively. (a) $H = -1.319 < E_{\text{thr}2}$ and the orbit cannot climb over SP2. (b,c) $E_{\text{thr}2} < H = -1.263 < E_{\text{thr}1}$ and the orbit can pass SP2, but cannot pass SP1. (d) $H = -1.011 > E_{\text{thr}1}$ and the orbit could climb over the SP1. Perturbation parameters in Eq. (11) are $\delta A_3 = 0.004528$ in (a) and $\delta A_3 = 0.032866$ in (b). Similarly, perturbations applied at site 1 are $\delta A_1 = 0.055125$ in (c) and $\delta A_1 = 0.158584$ in (d). In all the cases, $\lambda = 3$, $\varepsilon_1 = -0.5$, $\varepsilon_3 = 0$, $A_1^{\text{TDB}} = 0.1412$, $A_3^{\text{TDB}} = 0.1664$, and $\delta_\theta = \pi$.

which again gives rise to a TDB, with the norm (power) at site 1 larger than that in the symmetric case, see Fig. 2(f). In this case, the SP2 remains nearly unaffected, while SP1 moves towards the TDB, and the relationship between the energy thresholds is $E_{\text{thr}1} < E_{\text{thr}2}$. Note that, if ε_1 is small enough (i.e., $\varepsilon_1 \rightarrow -\infty$), SP1 will disappear and value $E_{\text{thr}1}$ cannot be reached, as shown in the Supplementary Figure 7(a) in our supplementary material (Appendix).

To study the transport of matter waves through the TDB in the opposite directions, we first consider the incident wave coming from the right. In terms of the trimer model, this may be considered as a case in which the stationary TDB is disturbed at site 3:

$$\psi_n(t=0) = \{A_1^{\text{TDB}}, A_2, (A_3^{\text{TDB}} + \delta A_3)e^{i\delta_\theta}\}, \quad (11)$$

with $A_2 = -\sqrt{1 - |\psi_1|^2 - |\psi_3|^2}$, perturbation amplitude δA_3 at site 3, and the corresponding phase by δ_θ . The resulting evolution of the trimer system, initiated by the perturbation, is shown by black trajectories in Fig. 3 for fixed $\lambda = 3$, $\varepsilon_1 = -0.5$, and $\varepsilon_3 = 0$, so that $E_{\text{thr}1} = -1.01787 > E_{\text{thr}2} = -1.29859$. If the perturbation is small, the total energy of the system, H , remains smaller than $E_{\text{thr}2}$, hence the orbit is not able to climb over saddle point SP2, while the TDB remains stable. That is, for this case nothing is transferred to site 1, as shown in Fig. 3(a). If the perturbation is large, so that

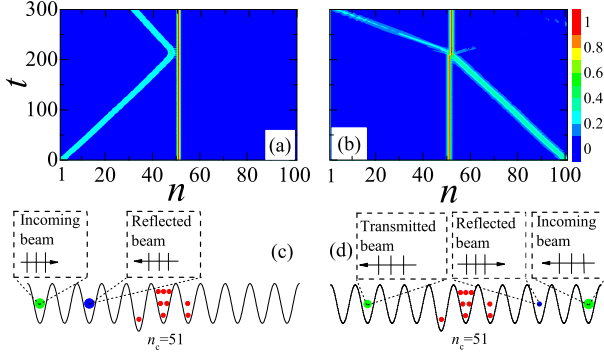


FIG. 4: (Color online) The transfer of incident waves through the stationary TDB in a long lattices ($M = 101$ sites), for the same excitation arriving from left in (a) and right in (b), respectively. Colors present the norms at the sites. In (c) and (d), the small and red circles depict the TDBs located, essentially, at sites 50, 51, and 52, with $A_{50} = 0.1502$, $A_{51} = 974553$, $A_{52} = 0.166384$. Circles of different size and color represent the incident, reflected, and transmitted excitations. The amplitudes of the incident excitations are $A_1 = A_4 = 0.2$ and $A_2 = A_3 = 0.4$, and its energy is $\delta E = 0.39743$. The energy thresholds are $E_{\text{thr1}} = -1.14325$ in (a) and $E_{\text{thr2}} = -1.30276$ in (b) for the excitations arriving from left and right, respectively. In all the cases, $\lambda = 3$ and $\varepsilon_n = 0$, except for $\varepsilon_{50} = -0.3$, and $E_{\text{TDB}} = -1.6573$.

$H > E_{\text{thr2}}$, the orbit can pass saddle point SP2, and a part of the norm (power) is transferred to site 1, as shown in Fig. 3(b).

If the incident wave comes from the left, it can be considered as the perturbation added to the stationary TDB at site 1. Then, one arrives at similar conclusions. First, if the perturbation is small, no transport takes place, as shown in Fig. 3(c). Next, if the perturbation is large, leading to $H > E_{\text{thr1}}$, a part of the norm (power) is transferred to site 3, as shown in Fig. 3(d).

Note that in Fig. 3(b) and (c) we have chosen the same initial conditions, i.e., there are the same energies of TDB, H , and the same incident excitations, coming from the opposite directions. Thus, it follows from the above considerations that, in the intermediate case,

$$E_{\text{thr2}} < H < E_{\text{thr1}}, \quad (12)$$

the transport from one side to the other can take place in Fig. 3(b), while it is forbidden in Fig. 3(c). That is, the same incident wave can pass from right to left, but *not* in the opposite direction, which implies non-reciprocal transmission.

Next, we have performed simulations of the transport of the incident waves in the full extended lattice of size $M = 101$ with the embedded TDB. The incident waves arrive from left and right to collide with the TDB, as shown in Fig. 4(c) and (d), respectively. Initially, the TDB is taken in the stationary form predicted by the trimer model, the respective energy thresholds being $E_{\text{thr1}} = -1.14325$ and $E_{\text{thr2}} = -1.30276$, with $\lambda = 3$, $\varepsilon_1 = -0.3$, $\varepsilon_3 = 0$, and $H_{\text{TDB}} = -1.6573$. The energy

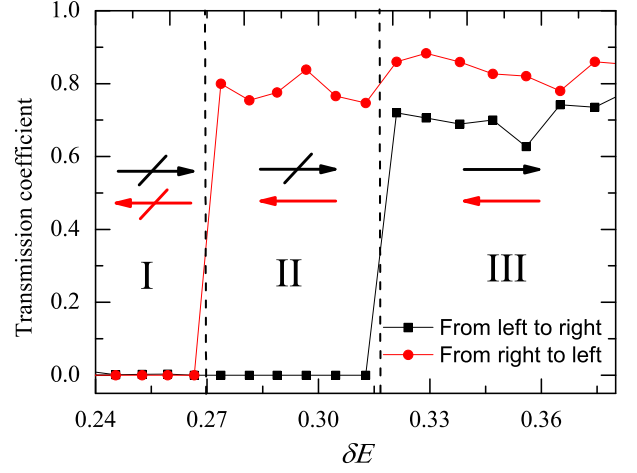


FIG. 5: (Color online) The transmission coefficient for the passage through the stationary TDB in the long lattice ($M = 101$ sites) of the same incident excitation arriving from left (squares and lines) and right (circles and lines), as a function of δE . The energy thresholds for the incoming beam from left and right satisfy $E_{\text{thr1}} > E_{\text{thr2}}$, and $\rightarrow (\nrightarrow)$ represents the incident wave can (cannot) pass the TDB. In region I: $E_t < E_{\text{thr2}}$; II: $E_{\text{thr2}} < E_t < E_{\text{thr1}}$; III: $E_t > E_{\text{thr1}}$. The TDB is located, essentially, at sites 50, 51, and 52, with $A_{50} = 0.163359$, $A_{51} = 972447$, and $A_{52} = 0.166316$, respectively. In all the cases, $\lambda = 3$ and $\varepsilon_n = 0$, except for $\varepsilon_{50} = -0.05$.

of the incident wave packets is $\delta E = 0.39743$, hence the total energy, including the TDB and the incident wave, is $E_t = H_{\text{TDB}} + \delta E$. In the simulations, we focus on the case of $E_{\text{thr2}} < E_t < E_{\text{thr1}}$, as Eq. (12) suggests that in this case the unidirectional transfer may be expected. The simulations confirm this expectation: while the wave arriving from the left is entirely reflected by the TDB, see Figs. 4(a) and (c), the one incident from the right is chiefly transmitted through the TDB, although a weak component is reflected, as seen in Figs. 4(b) and (d).

Collecting results of the systematic simulations for the full lattice, we conclude that the unidirectional transfer through the TDB (the “diode effect”) strongly depends on the total energy, E_t . Thus, δE may be used as an efficient control parameter to govern the outcome of the collision of the incident wave packet with the given TDB. To clearly display the results, in Fig. 5 we present the transmission coefficient for the passage of the left- and right-incident wave packets through the given TDB versus δE in the long lattices ($M = 101$ sites). In region I, $E_t < E_{\text{thr2}} < E_{\text{thr1}}$, the transmission coefficients for both the left- and right-incident waves are practically zero. In the middle region II, $E_{\text{thr2}} < E_t < E_{\text{thr1}}$, only the right-incident wave passes the TDB, while the left wave is reflected. The “diode effect” in region II can be controlled by adjusting ε_{n-1} and ε_{n+1} . Finally, in region III, $E_{\text{thr2}} < E_{\text{thr1}} < E_t$, the TDB is passable in both directions. In particular, if ε_{n-1} is small enough (i.e., $\varepsilon_{n-1} \rightarrow -\infty$), SP1 disappears [see Figure 6(a) in Sup-

plementary Material], and region III does not exist. In the latter case, the incident wave packets cannot pass the TDB from left to right, irrespective of δE , and the TDB acts as “full diode”.

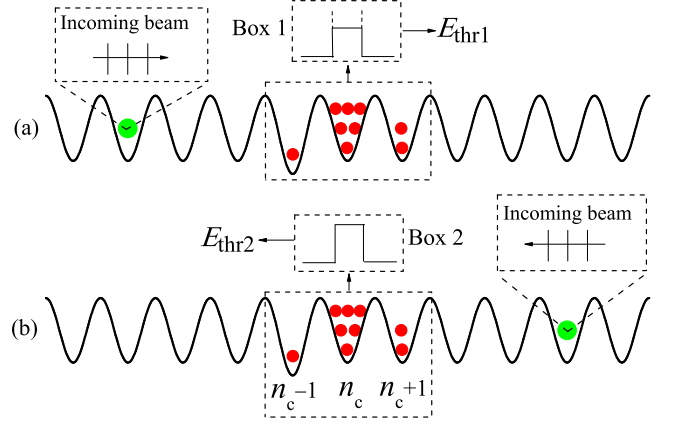
In conclusions, we have investigated the transport of small-amplitude waves through the TDB (tilted discrete breather) in the framework of the DNLS model with the asymmetric on-site defect potential. As a result, the diode-like transport mode has been found, i.e., the unidirectional transfer of the waves across the TDB, while the underlying lattice itself (without the TDB placed at a desired position) cannot operate in such a mode. The underlying mechanism was accurately explained in terms by the consideration of respective energy barriers. In the experimental realization of the system in BEC, the defect potential can be created, respectively, as a barrier or well, by a blue- or red-detuned laser beam illuminating the BEC at a particular site [52–54]. In terms of optical waveguide arrays, the potential can be induced by altering the effective refractive index in particular cores. The results suggest a scheme for the implementation of controlled blocking, filtering, and routing of matter-wave and optical beams in guiding networks. In particular, the scheme may be useful as a tool for steering the transmission of matter waves in interferometry and quantum-information processing [55]. In addition to working with the atom and optical beams, the present results may find applications in other contexts to which the DNLS model applies.

This work is supported by the National Natural Science Foundation of China under Grant No 11474026 and the Fundamental Research Funds for the Central Universities under Grant No. 2015KJJCA01.

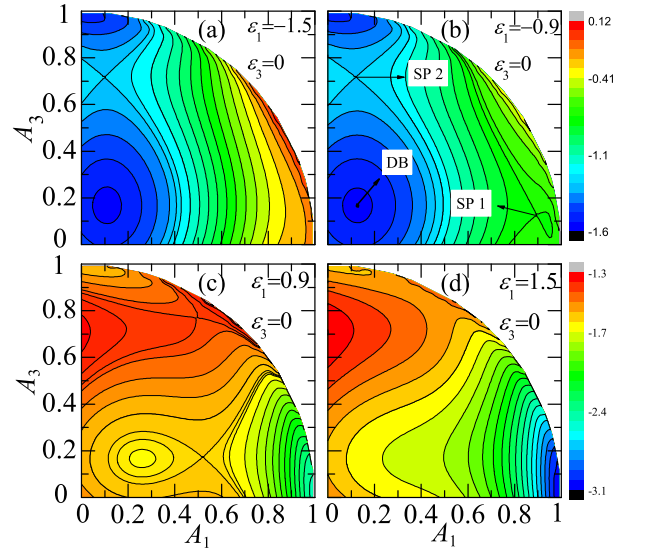
Appendix A: Supplementary material to main text

In the main text, we mainly consider the passage of wave packets in the opposite directions through the *tilted discrete breather* (TDB) pinned to the asymmetric local potential. As a result, we have found that the unidirectional passage (the “diode effect”) strongly depends on the total energy, E_t , and the threshold energies, $E_{thr1,2}$. As shown in Fig. 5 in the main text, if $E_t < E_{thr2} < E_{thr1}$, which is defined as region I, ($E_{thr2} < E_{thr1} < E_t$ in region III), the TDB is impassable (passable) for the wave packets arriving from either side. If $E_{thr2} < E_t < E_{thr1}$ (named region II), the incident wave pass the TDB unidirectionally (from right to left in Fig. 5 of the main text), with a high transmission coefficients. In this supplementary material, we discuss a particular case that ε_1 is very small (i.e., $\varepsilon_1 \rightarrow -\infty$) and large (i.e., $\varepsilon_1 \rightarrow +\infty$).

In the main text it has been demonstrated that the left- (right-) incident wave packet passes the TDB only when its energy exceeds E_{thr1} (E_{thr2}). That is, the TDB creates different potential barriers E_{thr1} and E_{thr2} for the



Supplementary Figure 6: (Color online) The transport scheme under the consideration. Boxes 1 and 2 denote thresholds E_{thr1} and E_{thr2} , which must be overcome by the same wave packet coming from left in (a) and from right in (b). In Box 1, E_{thr1} is effectively infinite when $\varepsilon_{n_{c-1}}$ is small enough, which is denoted by vertical dotted lines, as the respective saddle point does not exist. Here $\varepsilon_n = 0$ except for $\varepsilon_{n_{c-1}} \equiv \varepsilon_1 < 0$.



Supplementary Figure 7: (Color online) Contour plots of the energy given by Eq. (8) of main paper for small and large ε_1 with fixed $\lambda = 3$ and $\varepsilon_3 = 0$. SP1 and SP2 denote the saddle points.

same wave packet arriving from the different directions. This is illustrated by Supplementary Fig. 1.

The effect of ε_n on the Hamiltonian, considered as a function of A_1 and A_3 , is shown in Fig. 2(a)-(c) in the main text. When $\varepsilon_3 = 0$ and $\varepsilon_1 = -0.5$, the discrete soliton is a TDB, with $E_{thr1} > E_{thr2}$. In this case, although it is harder for the wave packet to pass the TDB from left to right, it still can do that at $E_t > E_{thr1}$. However, if ε_1 is very small, the energy at the saddle point SP1 is much higher than at SP2, i.e., $E_{thr1} \gg E_{thr2}$, as shown in

Supplementary Fig. 2(b). In particular, when ε_1 is small enough, SP1 disappears, and E_{thr1} becomes a value that can not be reached, as shown in Supplementary Fig. 2(a). Effectively, in the latter case, the TDB is an infinitely high potential barrier for the wave packet arriving from the left side, as depicted by the vertical dotted lines in the Box 1 in Supplementary Fig. 1(a). Hence, irrespective of E_t , the wave packet cannot pass the TDB from

left to right, making the TDB a full diode-like object.

On the other hand, when ε_1 is large enough, SP1 and DB disappear. Accordingly, the thresholds $E_{\text{thr1,2}}$ will also be meaningless, as shown in Supplementary Figs. 2(c) and (d). Lastly, the transfer of the wave packet through the TDB from right to left can be controlled by means of the potential parameter ε_3 .

-
- [1] A. J. Sievers and J. B. Page, in *Phonon Physics: The Cutting Edge, Dynamical Properties of Solids Vol. VII* (Elsevier, Amsterdam, 1995); S. Aubry, *Physica* (Amsterdam) **103D**, 201 (1997); S. Flach and C. R. Willis, *Phys. Rep.* **295**, 181 (1998); S. Flach and A. V. Gorbach, *ibid.* **467**, 1 (2008).
 - [2] P. G. Kevrekidis, *The Discrete Nonlinear Schrödinger Equation: Mathematical Analysis, Numerical Computations, and Physical Perspectives* (Berlin: Springer, 2009).
 - [3] M. Sato, B. E. Hubbard, and A. J. Sievers, *Rev. Mod. Phys.* **78**, 137 (2006).
 - [4] E. Trias, J. J. Mazo, and T. P. Orlando, *Phys. Rev. Lett.* **84**, 741 (2000).
 - [5] A. V. Ustinov, *Chaos* **13**, 716 (2003).
 - [6] D. N. Christodoulides and R. I. Joseph, *Opt. Lett.* **13**, 794 (1988).
 - [7] R. Morandotti, U. Peschel, J. S. Aitchison, H. S. Eisenberg, and Y. Silberberg, *Phys. Rev. Lett.* **83**, 2726 (1999).
 - [8] F. Lederer, G. I. Stegeman, D. N. Christodoulides, G. Assanto, M. Segev, and Y. Silberberg, *Phys. Rep.* **463**, 1 (2008); Y. V. Kartashov, V. A. Vysloukh, and L. Torner, *Progr. Opt.* **52**, 63 (2009); U. Röpke, H. Bartelt, S. Unger, K. Schuster, and J. Kobelke, *Appl. Phys. B* **104**, 481 (2011).
 - [9] F. Eilenberger, S. Minardi, A. Szameit, U. Röpke, J. Kobelke, K. Schuster, H. Bartelt, S. Nolte, A. Tünnermann, and T. Pertsch, *Opt. Express* **19**, 23171 (2011).
 - [10] U. T. Schwarz, L. Q. English, and A. J. Sievers, *Phys. Rev. Lett.* **83**, 223 (1999).
 - [11] M. Sato and A. J. Sievers, *Nature (London)* **432**, 486 (2004).
 - [12] A. Trombettoni and A. Smerzi, *Phys. Rev. Lett.* **86**, 2353 (2001); F. K. Abdullaev, B. B. Baizakov, S. A. Darmanyan, V. V. Konotop, and M. Salerno, *Phys. Rev. A* **64**, 043606 (2001); R. Carretero-González and K. Promislow, *Phys. Rev. A* **66**, 033610 (2002); G. I. Alfimov, P. G. Kevrekidis, V. V. Konotop, and M. Salerno, *Phys. Rev. E* **66**, 046608 (2002).
 - [13] B. Eiermann, T. Anker, M. Albiez, M. Taglieber, P. Treutlein, K. P. Marzlin, and M. K. Oberthaler, *Phys. Rev. Lett.* **92**, 230401 (2004); O. Morsch and M. Oberthaler, *Rev. Mod. Phys.* **78**, 179 (2006).
 - [14] V. A. Brazhnyi and V. V. Konotop, *Mod. Phys. Lett. B* **18**, 627 (2004).
 - [15] E. B. Kolomeisky and J. P. Straley, *Phys. Rev. B* **46**, 11749 (1992); E. B. Kolomeisky, T. J. Newman, J. P. Straley, and X. Qi, *Phys. Rev. Lett.* **85**, 1146 (2000).
 - [16] J. K. Xue and A. X. Zhang, *Phys. Rev. Lett.* **101**, 180401 (2008); A. X. Zhang and J. K. Xue, *Phys. Rev. A* **80**, 043617 (2009).
 - [17] M. G. Clerc, R. G. Elias, and R. G. Rojas, *Phil. Trans. R. Soc. London Ser. B* **369**, 412 (2011).
 - [18] P. C. Matthews and H. Susanto, *Phys. Rev. E* **84**, 066207 (2011).
 - [19] S. Flach and C. R. Willis, *Phys. Rep.* **295**, 181 (1998).
 - [20] J. D. Andersen and V. M. Kenkre, *Phys. Rev. B* **47**, 11134 (1993).
 - [21] M. Peyrard, T. Dauxois, H. Hoyet, and C. R. Willis, *Physica D* **68**, 104 (1993).
 - [22] R. S. MacKay and J. A. Sepulchre, *Physica D* **119**, 148 (1998).
 - [23] P. J. Martinez, M. Meister, L. M. Floria, and F. Falo, *Chaos* **13**, 610 (2003).
 - [24] G. P. Tsironis and S. Aubry, *Phys. Rev. Lett.* **77**, 5225 (1996).
 - [25] R. Livi, R. Franzosi, and G. L. Oppo, *Phys. Rev. Lett.* **97**, 060401 (2006).
 - [26] G. S. Ng, H. Hennig, R. Fleischmann, T. Kottos, and T. Geisel, *New J. Phys.* **11**, 073045 (2009).
 - [27] R. Franzosi, R. Livi, and G.-L. Oppo, *J. Phys. B* **40**, 1195 (2007).
 - [28] T. Schumm, S. Hofferberth, L. M. Andersson, S. Wildermuth, S. Groth, I. Bar-Joseph, J. Schmiedmayer and P. Krüger, *Nat. Phys.* **1**, 57 (2005).
 - [29] D. Jaksch, H. J. Briegel, J. I. Cirac, C. W. Gardiner, and P. Zoller, *Phys. Rev. Lett.* **82**, 1975 (1999).
 - [30] G. K. Brennen, C. M. Caves, P. S. Jessen, and I. H. Deutsch, *Phys. Rev. Lett.* **82**, 1060 (1999).
 - [31] J. K. Pachos and P. L. Knight, *Phys. Rev. Lett.* **91**, 107902 (2003).
 - [32] A. Kay, J. K. Pachos, and C. S. Adams, *Phys. Rev. A* **73**, 022310 (2006).
 - [33] S. Lepri and G. Casati, *Phys. Rev. Lett.* **106**, 164101 (2011); S. Lepri and B. A. Malomed, *Phys. Rev. E* **87**, 042903 (2013).
 - [34] K. Gallo, G. Assanto, K. R. Parameswaran, and M. M. Fejer, *Appl. Phys. Lett.* **79**, 314 (2001).
 - [35] M. Kulishov, J. M. Laniel, N. Bélanger, J. Azaña, and D. V. Plant, *Opt. Express* **13**, 3068 (2005); S. Ding and G. P. Wang, *Appl. Phys. Lett.* **100**, 51913 (2012).
 - [36] M. W. Feise, I. V. Shadrivov, and Y. S. Kivshar, *Phys. Rev. E* **71**, 037602 (2005).
 - [37] M. Scalora, J. P. Dowling, C. M. Bowden, and M. J. Bloemer, *J. Appl. Phys.* **76**, 2023 (1994).
 - [38] M. J. Ablowitz, C. W. Curtis, and Y.-P. Ma, *Phys. Rev. A* **90**, 023813 (2014); Z. Li, R.-X. Wu, Y. Poo, Z. F. Lin, and Q. B. Li, *J. Optics* **16**, 125004 (2014).
 - [39] S. Feng and Y. Wang, *Optical Materials* **35**, 1455 (2013); *Opt. Exp.* **21**, 220 (2013); A. Cicek and B. Ulug, *Appl. Phys. B - Lasers and Opt.* **113**, 619 (2013); L. H. Wang, X. L. Yang, X. F. Meng, Y. R. Wang, S. X. Chen, Z.

- Huang, and G. Y. Dong, Jpn. J. Appl. Phys. **52**, 122601 (2013); P. Wang, C. Ren, P. Han, and S. Feng, Opt. Mater. **46**, 195 (2015).
- [40] V. V. Konotop and V. Kuzmiak, Phys. Rev. B **66**, 14 (2002).
- [41] F. Biancalana, J. Appl. Phys. **104**, 093113 (2008).
- [42] J.-H. Wu, M. Artoni, and G. C. La Rocca, Phys. Rev. Lett. **113**, 123004 (2014); C. Sayrin, C. n Junge, R. Mitsch, B. Albrecht, D. OShea, P. Schneeweiss, J. Volz, and A. Rauschenbeutel, Phys. Rev. X **5**, 041036 (2015).
- [43] V. Grigoriev and F. Biancalana, Opt. Lett. **36**, 2131 (2011).
- [44] H. Ramezani, T. Kottos, R. El-Ganainy, and D. N. Christodoulides, Phys. Rev. A **82**, 043803 (2010); A. Regensburger, C. Bersch, M. A. Miri, G. Onishchukov, D. N. Christodoulides, and U. Peschel, Nature **488**, 167 (2012); M.-A. Miri, A. Regensburger, U. Peschel, and D. N. Christodoulides, Phys. Rev. A **86**, 023807 (2012); J. D'Ambroise, P. G. Kevrekidis, and S. Lepri, J. Phys. A: Math. Theor. **45**, 444012 (2012); J. D'Ambroise, S. Lepri, B. A. Malomed, and P. G. Kevrekidis, Phys. Lett. A **378**, 2824 (2014); J. Gear, F. Liu, S. T. Chu, S. Rotter, and J. S. Li, *ibid.* **91**, 033825 (2015); S. Yu, X. Piao, K. W. Yoo, J. Shin, and N. Park, Opt. Express **23**, 24997 (2015); Y. Jia, Y. Yan, S. V. Kesava, E. D. Gomez, and N. C. Giebink, ACS Photonics **2**, 319 (2015);
- [45] S. Kiriwara, M. W. Takeda, K. Sakoda, and Y. Miyamoto, Solid State Comm. **124**, 135 (2002).
- [46] F. Tao, W. Chen, W. Xu, J. T. Pan, and S. D. Du, Phys. Rev. E **83**, 056605 (2011).
- [47] P. W. Anderson, Phys. Rev. **109**, 1492 (1958).
- [48] J. Billy, V. Josse, Z. Zuo, A. Bernard, B. Hambrecht, P. Lugan, D. Clement, L. Sanchez-Palencia, P. Bouyer, and A. Aspect, Nature (London) **453**, 891 (2008).
- [49] L. Fallani, J. E. Lye, V. Guarrera, C. Fort, and M. Inguscio, Phys. Rev. Lett. **98**, 130404 (2007)
- [50] D. Jaksch, C. Bruder, J. I. Cirac, C. W. Gardiner, and P. Zoller, Phys. Rev. Lett. **81**, 3108 (1998).
- [51] H. Hennig, J. Dorignac, and D. K. Campbell, Phys. Rev. A **82**, 053604 (2010).
- [52] C. Fort, L. Fallani, V. Guarrera, J. E. Lye, M. Modugno, D. S. Wiersma, and M. Inguscio, Phys. Rev. Lett. **95**, 170410 (2005).
- [53] J. E. Lye, L. Fallani, M. Modugno, D. S. Wiersma, C. Fort, and M. Inguscio, Phys. Rev. Lett. **95**, 070401 (2005).
- [54] A. Trombettoni, A. Smerzi, and A. R. Bishop, Phys. Rev. Lett. **88**, 173902 (2002)
- [55] R. A. Vicencio, J. Brand, and S. Flach, Phys. Rev. Lett. **98**, 184102 (2007).